ACS OMEGA

http://pubs.acs.org/journal/acsodf

Article

Assay Performance of a Label-Free, Solution-Phase CYFRA 21-1 Determination

Amanda K. Kussrow, Michael N. Kammer, Pierre P. Massion, Rebekah Webster, and Darryl J. Bornhop*

Cite This: *ACS Omega* 2022, 7, 31916−31923

Read Online

ACCESS | Metrics & More | Article Recommendations

ABSTRACT: CYFRA 21.1, a cytokeratin fragment of epithelial origin, has long been a valuable blood-based biomarker. As with most biomarkers, the clinical diagnostic value of CYFRA 21.1 is dependent on the quantitative performance of the assay. Looking toward translation, it is shown here that a free-solution assay (FSA) coupled with a compensated interferometric reader (CIR) can be used to provide excellent analytical performance in quantifying CYFRA 21.1 in patient serum samples. This report focuses on the analytical performance of the high-sensitivity (hs)-CYFRA 21.1 assay in the context of quantifying the biomarker in two indeterminate pulmonary nodule (IPN) patient cohorts totaling 179 patients. Each of the ten assay calibrations consisted of 6 concentrations, each run as 7 replicates (e.g., 10 × 6 × 7 data points) and were performed on two different instruments by two different operators. Coefficients of variation (CVs) for the hs-CYFRA 21.1 analytical figures of merit, limit of quantification (LOQ) of ca. 60 pg/mL, B_{max}, initial slope, probe−target binding affinity, and reproducibility of quantifying an unknown were found to range from 2.5 to 8.3%. Our results demonstrate the excellent performance of our FSA-CIR hs-CYFRA 21-1 assay and a proof of concept for potentially redefining the performance characteristics of this existing important candidate biomarker.

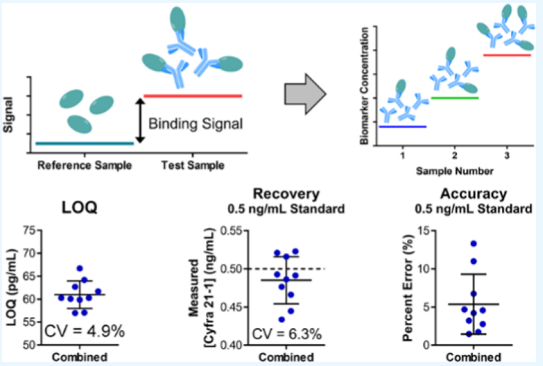

INTRODUCTION

The quantification of protein biomarkers at physiologically relevant levels in patient serum samples is essential across the continuum of patient care, from diagnostics to response to therapy. Among the major contributors to the clinical translation bottleneck for biomarker assays is the intrinsic biological variability in large cohorts of samples for systemic biomarkers, the relatively long development time for assays, and the need for assays with improved sensitivity.[1]

Many approaches exist to quantify biomarkers at high sensitivity, with most depending heavily on the ability to quantify molecular interactions. These include enzyme-linked immunosorbent assay (ELISA), bead array technologies, and mass spectrometry (MS).[2−8] Some new methods report single-molecule sensitivity[9] and, as we have shown,[10] have the potential to impact clinical practice due to their low limit of quantification (LOQ).[11] While the free-solution assay (FSA), combined with the compensated interferometric reader (CIR), is not a single-molecule approach, it does represent a simpler (mix-and-read, label-free) approach to obtain picogram/mL sensitivity.[10] "Single molecule" techniques employ a fluorescence assay based on multiple chemical steps and relatively complicated optical readers. In Singulex, the probe volume is limited to a few femtoliters in a manner similar to confocal microscopy. Combining this optical approach with a fluorescent sandwich assay that uses a capture and separation step provides excellent signal-to-noise (S/N).[9] The Simoa (Single-Molecule Array) from Quanterix technology exploits the advantages of digital assays by employing fluorescence-labeled sandwich beads, which are each collected in wells formed at the end of a coherent fiber optic or similar small volume receptacle.[12,13] Both of these techniques are promising but still are somewhat limited by speed, reproducibility, cost, and/or accessibility.

SOMALOGIC has taken a different approach to quantify serum proteins by employing aptamers (strands of DNA or RNA).[14] Their detection approach capitalizes on a slow "off-rate" for one of the protein−aptamer complexes formed to help separate the sample from the background.[15] This aptamer-probe method has shown promise for high-sensitivity (hs) protein quantification,[16] yet multiple (ca. 10) sample handling and labeling steps, combined with relatively complicated instrumentation, have impeded the wide dissemination of the technology for biomarker quantification.

Received: May 4, 2022
Accepted: June 27, 2022
Published: August 29, 2022

Label-free techniques such as surface plasmon resonance (SPR), quartz crystal microbalance, wave-guided interferometry, and mass spectrometry (MS) have been used for biomarker quantification.[17−19] While MS has been exceedingly valuable in the biomarker discovery phase,[20−23] relative instrument complexity and difficulty with quantification make its use in clinical validation unattractive. Multiplexed MRM/MS targeted assays using stable isotope-labeled peptide standards for quantitation show promise as clinical diagnostic assays, yet low-throughput remains a challenge.[23−25]

In label-free methods, surface immobilization can negatively influence assay development time and sensitivity in complex matrices.[26−29] Actually, the same is true for the most common methods used today for biomarker analysis, such as ELISA and/or bead arrays, which also require chemical modification for surface immobilization and/or labeling steps that can influence assay performance. Significant strides have been made toward miniaturizing, multiplexing, and improving ELISA-like assays.[13,30] One example is the electrochemiluminescent (ECL) assay, which is typically 10-fold more sensitive than the standard fluorescent analogue.[31] Yet, reaching low picomolar or high femtomolar detection limits often requires amplification chemistries that can be costly and require lengthy development times. These limitations tend to extend the interval between biomarker discovery and clinical validation. Furthermore, the large sample consumption associated with some of these methods impedes validation of promising biomarkers due to the precious nature of banked samples on relevant patient populations. Therefore, the volume-constrained, FSA method represents an attractive alternative to ELISA.

Sensitivity and specificity of all interaction-based determinations are influenced by numerous factors. These include the equilibrium binding affinity, the transduction mechanism, and the level of background (matrix and/or spectroscopic). In general, the higher the magnitude of the equilibrium binding affinity (the lower the true-K_D), the lower the potential limit of detection. In fluorescence and absorbance determinations, performance is also impacted by quantum efficiencies, molar absorptivity, Stokes shifts, and other nonspectroscopic metrics for the analyte. FSA is therefore a complementary approach, with the signal transduction parameter dictating assay performance and the magnitude of change in dipole moment (e.g., refractive index, RI) due to conformation/hydration changes during the binding event.

Since lung cancer is the leading cause of cancer-related deaths in the United States, there is a growing movement to improve diagnostics. One approach is to implement low-dose chest computed tomography (CT) screening into routine practice. CT screening has been endorsed by U.S. Preventive Services Task Force, the American Thoracic Society, the American College of Chest Physicians, and reimbursement payers. While these programs can reduce lung cancer-specific mortality by 20% and overall mortality by 6.9% in high-risk individuals, numerous challenges still exist to realize early detection and better outcomes for the majority of lung cancer patients. Improved biomarker assays could address these challenges. So, (a) how to position biomarker use prior to or alongside chest CT screening to decrease the cost and rates of false-positive tests, and (b) how to diagnose lung cancer patients with indeterminate pulmonary nodules (IPNs)?

Recently, as with the development of the high-sensitivity (hs)-CRP assay for C-reactive protein (CRP),[32] we postulated that lowering the LOQ for CYFRA 21.1 can improve risk stratification within the context of noninvasive diagnosis of IPNs.[10,33] FSA-CIR represents the only solution-phase, label-free molecular interaction measurement methodology with sensitivity comparable to or better than fluorescence[10,34,35] that is compatible with a wide range of complex matrices,[36−38] and that offers good throughput and constrained sample consumption.[10,34] FSA-CIR can be used to address numerous previously challenging or intractable problems, ranging from poor *in vitro in vivo* correlations for first in human dosing[38] to the rapid quantification of low abundance chemicals in human samples, including neonatal opioids in urine and chemical nerve agents in urine and serum.[34,35] Capitalizing on the unique properties of FSA-CIR, we demonstrated a ∼10-fold LOQ improvement over ECL for the biomarker CYFRA 21.1.[10] This observation led to a larger study that showed there is promise for improving management of patients with IPNs using a CYFRA 21.1 assay, with improved LOQs.[33]

Here, we report on the long-term analytical performance of using the FSA and CIR[34,35,39] for quantifying CYFRA 21.1 in serum. We illustrate that CVs for the analytical figures of merit of the CYFRA 21.1 assay, LOQ, B_{max}, initial slope, probe−target apparent binding affinity, and reproducibility of quantifying an unknown range from 2.5 to 8.3%. These metrics of performance were obtained over the course of 16 days, with experiments run on 5 days while constructing 10 calibration curves and analyzing 2 unknowns (operator-blinded spiked samples) per calibration curve. The calibration tests were run in the context of studying two IPN patient cohorts, totaling 179 patients. Interestingly, our results came from a nanoliter-volume, universal, mix-and-read, solution-phase, enzyme amplification-free assay method that exhibits no relative mass sensitivity on serum and uses a reader with a simple optical train that does not require high-resolution temperature control.[39] These collective properties could pave the way for the use of FSA-CIR in the management of IPN patients in a clinical lab or the near-patient setting.

MATERIALS AND METHODS

The Assay methodology has been described in detail previously[10] and is described briefly here. The measurements were performed on the compensated interferometer, as described previously.[34,39−41] All lab disposables were purchased from Thermo Fisher Scientific, and reagents were purchased from Sigma-Aldrich. All aqueous solutions were prepared using deionized water. Pooled human serum was purchased from Valley Biomedical (Winchester, VA). The protein standard (CYFRA 21-1) was purchased from DRG International (Springfield, NJ). A CYFRA 21-1 monoclonal antibody (clone XC4, product #MBS850246) obtained from MyBioSource (San Diego, CA) was used as the probe.

Assay Preparation. Calibration solutions were prepared by spiking several aliquots of a 50% pooled human serum/50% phosphate-buffered saline (PBS) solution with concentrations of the biomarker target CYFRA 21-1 ranging from 0.08 to 25 ng/mL. To produce the binding sample, 20 μL of each serum aliquot was combined with 20 μL of a solution containing 2 μg/mL of the probe antibody. To produce an RI-matched, nonbinding reference sample, 20 μL of each serum aliquot was combined with 20 μL of a blank solution containing PBS devoid of antibodies. Final sample compositions were 25% serum in PBS, with CYFRA 21-1 concentrations of 0, 0.04, 0.10, 0.50, 2.50, and 12.50 ng/mL. The binding samples

https://doi.org/10.1021/acsomega.2c02763
ACS Omega 2022, 7, 31916−31923

contained 1 μg/mL of the probe antibody, and the reference samples were devoid of the probe.

Following a 1 h incubation at ambient temperature (22 °C) on a shaker (300 rpm), the sample and reference solutions were loaded onto the droplet generator in the order of increasing concentration and the phase shift between reference and binding samples was measured by the CIR. A calibration curve was created by fitting the resulting phase shift to a single site saturation isotherm according to the equation $Y = B_{max} \times X/(K_D + X)$, where Y is the phase shift at the concentration of X (in ng/mL). B_{max} and K_D are fitted to the data by nonlinear regression, where B_{max} is the maximum signal at saturation and K_D is the apparent dissociation constant. The initial slope of the calibration curve was determined by dividing B_{max} by K_D. The initial slope was used to calculate the assay limit of detection by 3 × (standard deviation of 5 s instrument baseline)/(initial slope), and the assay limit of quantification by 3 × (standard deviation of replicate measurements of the same sample)/(initial slope). The value used for X was taken as the final CYFRA 21-1 concentration in 25% serum (listed above) multiplied by 4 to recover the concentration of CYFRA 21-1 in 100% serum. This calibration curve was prepared from stock reagents independently for each assay.

Recovery was assessed by preparing spiked "unknowns." These test samples were prepared by adding a known quantity of the CYFRA 21-1 to pooled serum and then processing the samples, as described above. The biomarker concentration was recovered by fitting the signal to the calibration curve.

RESULTS AND DISCUSSION

The high-sensitivity analysis of serum protein reported here is enabled by marrying two synergistic technologies, a solution-phase assay and a compensated interferometer. CIR, shown in Figure 1 and described in detail elsewhere,[34,35,39,41] consists of three components, an optical engine, a droplet generator, and a syringe pump. The optical engine has a diode laser, an object

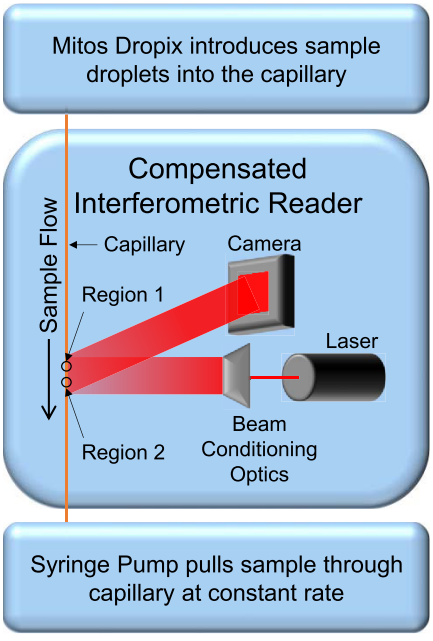

Figure 1. Block diagram CRI, illustrating sample flow from the droplet generator (top) through the laser and fringe detector (center) and to the syringe pump (bottom).

(polyimide-coated fused silica capillary tube, 250 × 350 μm), and a camera (Figure 1). Two nearly identical interferometers[41] result from spreading out the interrogation beam along the capillary and reading adjacent regions of the resulting interference fringes. The difference measurement facilitates high-resolution, low-volume refractive index (RI) measurements. Proper laser−capillary alignment and fringe pattern selection allow the elimination of the high-resolution temperature controller typically needed for such devices.[41] The relative RI measurement of reference-and-sample droplet pairs, separated by a 40 nL oil droplet, is accomplished by measuring positional fringe shifts in adjacent windows with a Fourier transform.[40,42] The fast Fourier transform (FFT) readout reports the positional fringe shift as a phase change. The polyimide-coated capillary tube serves as the main optical component of the optical train while providing seamless droplet train transfer. Use of a capillary is noteworthy because it provides improved sensitivity and S/N over chip-based optics.[43,44]

Use of a modified droplet generator (Mitos Dropix) upstream and a syringe pump (Harvard Apparatus, Holliston, Massachusetts) downstream from the compensated interferometer allows for the smooth introduction of the sample−reference droplet train. To mitigate nonspecific adsorption and reduce noise due to plastic leaching, sample well plates were made of highly biocompatible poly(ethyl ethyl ketone) (PEEK) resin.

Accurate patient CYFRA 21.1 quantification is contingent on having high-quality, reproducible, free-solution assay calibrations. These calibration curves provide analytical figures of merit, including the response function of the instrument and the quality of the assay chemistry. These standards are performed throughout the day intermixed with the patient's CYFRA determinations. Such a procedure ensures performance stability throughout determinations, mitigates bias, and has been described previously.[10]

Sensing of adjacent sample−reference droplets in a train provides numerous advantages, including complex matrix compatibility (specificity) and sensitivity that rival or exceed fluorescent assays.[41,45] Figure 2 illustrates the FSA biomarker workflow. A small volume of serum is split into two aliquots and then processed to provide "binding" and "reference" solutions. To quantify a biomarker target, we add an excess antibody probe to one of these aliquots, giving the "binding/test" sample. To the other aliquot, we add an RI matching solution without the probe. These solutions equilibrate for ∼1 h and are then introduced into adjacent wells of the droplet generator for analysis by the interferometer (as pairs separated by an oil droplet). The difference in signal between the sample−reference pair provides a quantitative measure of the antibody-target complex while allowing the matrix signal to be nullified. As previously described,[40] the scientific principle for FSA depends on binding-induced changes in molecular conformation and hydration, producing predictable and reproducible changes to the solution RI.

Our evaluation of the analytical performance of the CYFRA 21-1 assay in 25% serum is presented in the context of evaluating IPN patient samples.[33] We employed a commercial antibody (Ab) to the target biomarker, CYRFA 21.1 (MyBioSource, San Diego). Characterization and selection of this Ab involved a simple screening experiment with several Ab's, as described in detail elsewhere.[10,34,35,46] This experiment allows confirmation of antibody-target binding and signal-to-

https://doi.org/10.1021/acsomega.2c02763
ACS Omega 2022, 7, 31916−31923

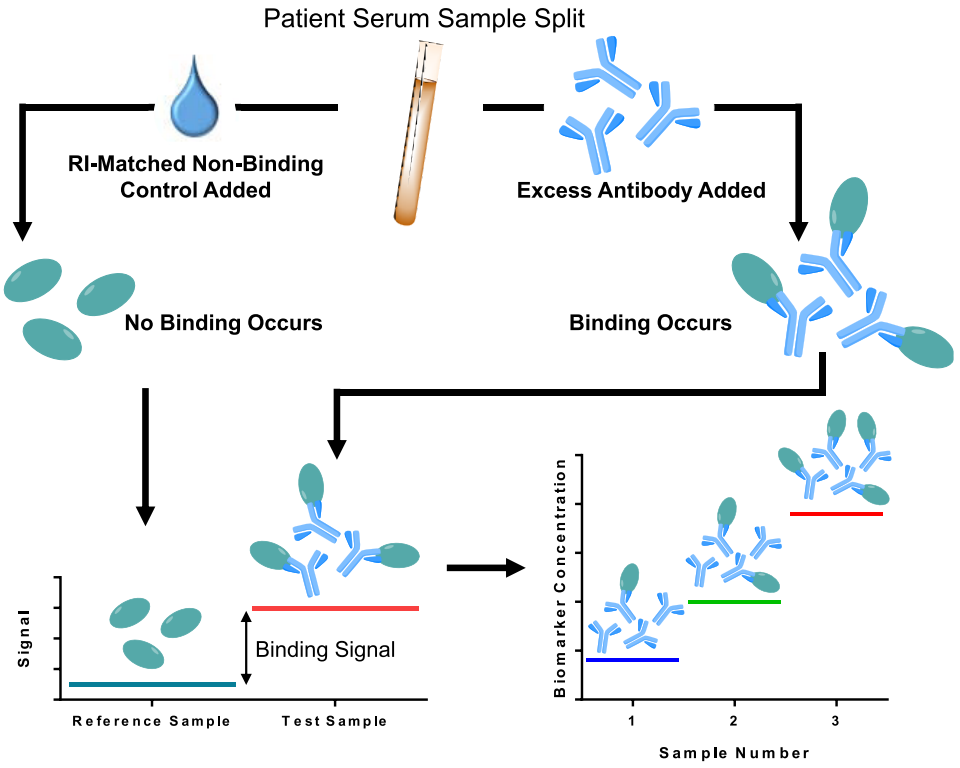

Figure 2. Schematic of the free-solution assay method.

noise (S/N) maximization. Once selected, the Ab is further characterized with a saturation isotherm determination to evaluate the quality of the molecular interaction and the binding affinity and obtain an estimate of the LOQ. While true-K_D determinations are used to "guide chemistry selection" during the assay development phase, our binding assay calibration curve represents an apparent K_D (app-K_D). This parameter serves both to define the response function for the assay and as a proxy for the fidelity of the molecular interaction or K_D (affinity). Hence, the app-K_D is obtained from calibrations and used as a key analytical figure of merit for the assay chemistry performance. Unlike fluorescence or absorption measurements, FSA transduces the molecular interaction between the probe and the target directly. Therefore, any variation or reduction in apparent binding affinity can influence the S/N for quantifying the target. Thus, the app-K_D obtained from response curve measurements provides a metric of probe Ab and target/standard quality. A full calibration curve (including unknowns) is performed with each batch of about 20 patient serum samples that are processed.

Accurate quantification of any analyte, regardless of the method, requires the determination of the instrumental response as a function of target concentration, preferably in the matrix of interest. FSA is no different. In the case of FSA-CIR, calibration curves are built in the target matrix and analyzed as sample and reference droplet trains. Specifically, samples of 25% serum containing 80 pg/mL to 50 ng/mL of the target protein (CYFRA 21-1) and the probe antibody are analyzed by comparing the response vs matrix-matched reference droplets and those consisting of identical concentrations of CYFRA 21-1 without the Ab (Figure 2).

Figure 3 presents a summary of 10 calibration determinations performed in 25% serum using CYFRA 21.1 standards

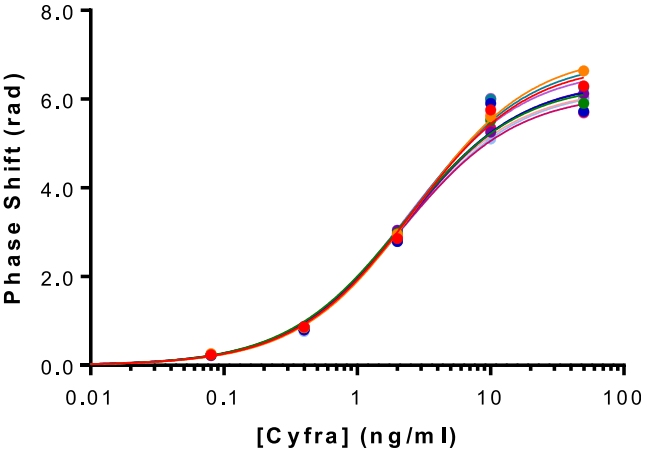

Figure 3. Representative replicate response function/app-K_D curve. Antibody at 1 μg/mL. Error bars representing the standard deviations for 6 determinations are present but not legible.

and an excess of antibody probe. Figure 3 illustrates the high quality and reproducibility of CYFRA 21.1 calibration curves run on FSA-CIR over multiple days with two different operators working with two different instruments. In the context of quantifying the CYFRA 21.1 protein biomarker in two patient cohorts, the FSA-CIR calibration methodology reported an average LOQ of 61 pg/mL with a standard deviation of 3.0 pg/mL for 10 determinations with 6 droplets at 6 concentrations. Correlation coefficients for these calibration curves ranged from an $R2$ = 0.981 to 0.999.

Assay accuracy/recovery is validated by preparing two unknowns with every calibration curve. These samples are made by spiking serum with CYFRA 21-1, blinding the instrument operator to sample identity and experimentally determining the biomarker concentration. Figure 4 shows that

https://doi.org/10.1021/acsomega.2c02763
ACS Omega 2022, 7, 31916−31923

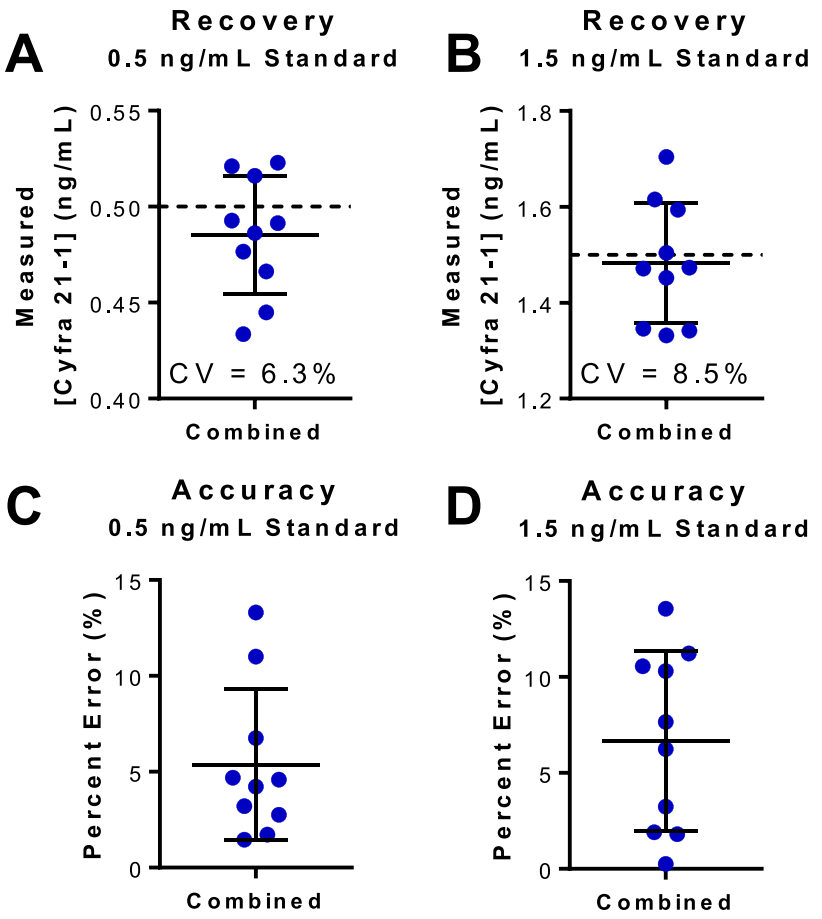

Figure 4. Plot (A) and (B) present the recovery values and, (C) and (D), the accuracy (percent error) for quantifying CYFRA 21-1 with FSA-CIR.

FSA-CIR provides excellent recovery at both 500 pg/mL and 1.5 ng/mL. The results demonstrate the method is highly accurate and quantitative, with the error in correctly determining the CYFRA 21.1 concentration ranging from 0.25 to 13.6% for unknowns. Overall, within the operating range of the calibration curve (80 pg/mL to 10 ng/mL), FSA-CIR provided an average percent difference between actual and determined concentration (recovery level) of 6.02%.

Further evidence of the performance of FSA-CIR is seen in the LOQ data. As shown in Figure 5A, the LOQ of the 10 calibration determinations, run in the context of patient sample determinations, ranged from 57.0 to 66.7 pg/mL, giving a CV of 4.9%. These LOQ values are ∼1.5-fold better than the LOQ of 80 pg/mL,[47] published recently for a somewhat complicated, chemically intensive immunoassay, and ∼10-fold better than the ∼500 pg/mL LOQ for the commercial, gold standard Roche Cobas electro-chemiluminescence assay (ECLIA) for CYFRA 21-1.[48]

Additional analytical FOM measurements for the 10 calibrations (two independent instruments and operators) performed on 5 subsequent days in 25% serum are extracted from the calibration curves. These metrics include the B_{max} (Figure 5B), app-K_D (Figure 5C), pooled standard deviation (Figure 5D), initial slope (Figure 5E), and the correlation coefficient (Figure 5F). Here, for ten discrete determinations, maximum response, B_{max}, ranged from 6141 milliradians to 7044 milliradians, exhibiting a CV of 4.7%. The initial slope for the FSA-CIR calibration curves was found to be 2582 mrad/ng/mL to 2948 mrad/ng/mL, with a CV of 4.1%, and the app-

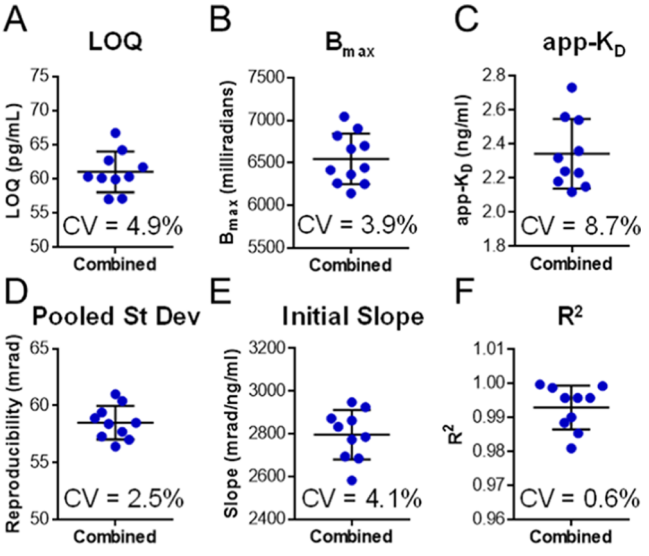

Figure 5. Summary of the assay figures of merit: (A) Limit of quantification, (B) saturation binding signal, (C) apparent K_D, (D) pooled standard deviation, (E) initial slope of the saturation isotherm, and (F) correlation coefficient.

K_D spanned from 2.12 to 2.73 ng/mL, with a CV of just 8.7%. The pooled standard deviation of the calibration measurements was determined to be 56.4−61.0 mrad, with a CV of only 2.5%. It is noteworthy that each data point displayed in Figure 5 represents an entire calibration run consisting of 6

https://doi.org/10.1021/acsomega.2c02763
ACS Omega 2022, 7, 31916−31923

sample and reference pair measurements at each of 6 concentrations (including a zero value).

DISCUSSION

In this report, it was shown that a mix-and-read, free-solution assay combined with a compensated interferometer enables the quantification of CYFRA 21.1 in serum samples by two independent instruments/operators over the course of 16 days, with 5 days of experimentation. The result was excellent LOQs, precision, and accuracy. The assay employs a single monoclonal antibody (IgG1 anti-CK19 clone XC4 (MyBioSource, San Diego, CA)) and capitalizes on a unique label-free, signal transduction method based on binding-induced solution-phase conformation and hydration changes the free-solution response function (FreeSRF).[40] FSA is label-free (no fluorescence or radiolabeling), making it rapid, cost-effective, and allowing the use of unaltered or minimally processed patient samples. It is also assay agnostic, allowing for quantitation of a wide array of interactions (antibodies to DNA to small molecules) in a mass-independent manner.

The compensated interferometer is a unique biosensor that capitalizes on an adjacent sample−reference configuration for matrix-insensitive operation and assay specificity. Analysis can be effectively performed on constrained volumes (<10 μL of patient serum), facilitating multiple replicates to be performed on quantity-limited samples. The optical engine of CIR is simple, consisting of a diode laser, a capillary tube, and a camera. CIR is also among the most sensitive nanoliter-volume universal sensors. Under conditions reported here, the instrument performed at a baseline noise level of $<10^{-7}$ RIU, enabling a LOQ for CYFRA 21.1 of 61 pg/mL in 25% serum. At this LOQ, in the probe volume of 40 nL defined by the laser−capillary interaction, there is just 610 attograms (~4 zeptomoles) of the target-probe present. Overall, FOM CVs range from 2.5 to 8.7%, with no CV exceeding 9%.

The data shown here was generated in the context of an ongoing multisite prospectively collected, retrospective blinded evaluation (PROBE) design trail[49] to determine the clinical utility of adding hs-CFRA 21.1 by FSA-CIR as a biomarker to the clinical problem of discrimination of cases from controls in lung cancer patients with indeterminate pulmonary nodules (IPNs).[33] Here, our focus was on the analytical performance of the assay methodology to demonstrate that a manual, first-generation prototype instrument provides excellent performance over multiple days of biomarker analysis research. We are acutely aware that to have an ongoing impact in the clinical setting, refinement of our instrument and assay will be necessary. Thus, to enable FSA-CIR translation, we are currently working on a next-generation CIR with full automation, from alignment to data analysis. Should our approach withstand more stringent validation, FSA-CIR could provide improved noninvasive testing for the clinical management of patients with lung cancer and other diseases.

The unique nature of FSA also represents numerous opportunities to rapidly develop and characterize new assays. For example, preliminary validation tests look promising for using FSA-CIR to quantify the serum biomarkers HE-4 and CEA. Further, because FSA is assay agnostic, various types of probes, including DNA/RNA aptamers and small molecules, all represent opportunities.[34,35] The unique transduction method of FSA could represent a way forward in reducing the biomarker validation bottleneck and expediting the clinical translation of new biomarkers of disease.

AUTHOR INFORMATION

Corresponding Author

Darryl J. Bornhop − *Department of Chemistry and The Vanderbilt Institute for Chemical Biology, Vanderbilt University, Nashville, Tennessee 37235, United States*; Email: Darryl.bornhop@vanderbilt.edu

Authors

Amanda K. Kussrow − *Department of Chemistry and The Vanderbilt Institute for Chemical Biology, Vanderbilt University, Nashville, Tennessee 37235, United States*; orcid.org/0000-0002-0423-2066

Michael N. Kammer − *Division of Allergy, Pulmonary and Critical Care Medicine and Vanderbilt-Ingram Cancer Center, Vanderbilt University, Nashville, Tennessee 37235, United States*; orcid.org/0000-0001-7912-8450

Pierre P. Massion − *Division of Allergy, Pulmonary and Critical Care Medicine and Vanderbilt-Ingram Cancer Center, Vanderbilt University, Nashville, Tennessee 37235, United States*; orcid.org/0000-0003-0647-0559

Rebekah Webster − *Department of Chemistry and The Vanderbilt Institute for Chemical Biology, Vanderbilt University, Nashville, Tennessee 37235, United States*

Complete contact information is available at: https://pubs.acs.org/10.1021/acsomega.2c02763

Notes

The authors declare no competing financial interest.

ACKNOWLEDGMENTS

For Pierre, who was a true believer in the potential of "BSI," his presence and collaborative contributions will be sorely missed. Funding: Part of this study was funded by CA186145 and CA152662 awarded to P.P.M., NSF CHE-1610964 awarded to D.J.B., and the Lung Cancer Research Foundation awarded to A.K.K.

REFERENCES

(1) Mazzone, P. J.; Sears, C. R.; Arenberg, D. A.; Gaga, M.; Gould, M. K.; Massion, P. P.; Nair, V. S.; Powell, C. A.; Silvestri, G. A.; Vachani, A.; Wiener, R. S. Oncology, A. A. T., Evaluating Molecular Biomarkers for the Early Detection of Lung Cancer: When Is a Biomarker Ready for Clinical Use? An Official American Thoracic Society Policy Statement. *Am. J. Respir. Crit. Care Med.* **2017**, *196*, E15−E29.

(2) Wang, J.; Ahmad, H.; Ma, C.; Shi, Q. H.; Vermesh, O.; Vermesh, U.; Heath, J. A self-powered, one-step chip for rapid, quantitative and multiplexed detection of proteins from pinpricks of whole blood. *Lab Chip* **2010**, *10*, 3157−3162.

(3) Fan, R.; Vermesh, O.; Srivastava, A.; Yen, B. K. H.; Qin, L. D.; Ahmad, H.; Kwong, G. A.; Liu, C. C.; Gould, J.; Hood, L.; Heath, J. R. Integrated barcode chips for rapid, multiplexed analysis of proteins in microliter quantities of blood. *Nat. Biotechnol.* **2008**, *26*, 1373−1378.

(4) Garcia-Cordero, J. L.; Maerkl, S. J. A 1024-sample serum analyzer chip for cancer diagnostics. *Lab Chip* **2014**, *14*, 2642−2650.

(5) Lee, H. J.; Kim, Y. T.; Park, P. J.; Shin, Y. S.; Kang, K. N.; Kim, Y.; Kim, C. W. A novel detection method of non-small cell lung cancer using multiplexed bead-based serum biomarker profiling. *J. Thorac. Cardiovasc. Surg.* **2012**, *143*, 421−U447.

(6) Lee, H. J.; Nedelkov, D.; Corn, R. M. Surface plasmon resonance imaging measurements of antibody arrays for the multiplexed detection of low molecular weight protein biomarkers. *Anal. Chem.* **2006**, *78*, 6504−6510.

https://doi.org/10.1021/acsomega.2c02763
ACS Omega 2022, 7, 31916−31923

(7) Teramura, Y.; Iwata, H. Label-free immunosensing for alpha-fetoprotein in human plasma using surface plasmon resonance. *Anal. Biochem.* **2007**, *365*, 201−207.
(8) Guerra, E. N. S.; Rego, D. F.; Elias, S. T.; Coletta, R. D.; Mezzomo, L. A. M.; Gozal, D.; Canto, G. D. Diagnostic accuracy of serum biomarkers for head and neck cancer: A systematic review and meta-analysis. *Crit. Rev. Oncol. Hematol.* **2016**, *101*, 93−118.
(9) Gilbert, M.; Livingston, R.; Felberg, J.; Bishop, J. J. Multiplex single molecule counting technology used to generate interleukin 4, interleukin 6, and interleukin 10 reference limits. *Anal. Biochem.* **2016**, *503*, 11−20.
(10) Kammer, M. N.; Kussrow, A. K.; Webster, R. L.; Chen, H. D.; Hoeksema, M.; Christenson, R.; Massion, P. P.; Bornhop, D. J. Compensated Interferometry Measures of CYFRA 21-1 Improve Diagnosis of Lung Cancer. *ACS Comb. Sci.* **2019**, *21*, 465−472.
(11) Hori, S. S.; Gambhir, S. S. Mathematical Model Identifies Blood Biomarker−Based Early Cancer Detection Strategies and Limitations. *Sci. Transl. Med.* **2011**, *3*, 109−116.
(12) Rissin, D. M.; Kan, C. W.; Campbell, T. G.; Howes, S. C.; Fournier, D. R.; Song, L.; Piech, T.; Patel, P. P.; Chang, L.; Rivnak, A. J.; Ferrell, E. P.; Randall, J. D.; Provuncher, G. K.; Walt, D. R.; Duffy, D. C. Single-molecule enzyme-linked immunosorbent assay detects serum proteins at subfemtomolar concentrations. *Nat. Biotechnol.* **2010**, *28*, 595−599.
(13) Rissin, D. M.; Kan, C. W.; Song, L. N.; Rivnak, A. J.; Fishburn, M. W.; Shao, Q. C.; Piech, T.; Ferrell, E. P.; Meyer, R. E.; Campbell, T. G.; Fournier, D. R.; Duffy, D. C. Multiplexed single molecule immunoassays. *Lab Chip* **2013**, *13*, 2902−2911.
(14) Gold, L.; Ayers, D.; Bertino, J.; Bock, C.; Bock, A.; Brody, E. N.; Carter, J.; Dalby, A. B.; Eaton, B. E.; Fitzwater, T.; Flather, D.; Forbes, A.; Foreman, T.; Fowler, C.; Gawande, B.; Goss, M.; Gunn, M.; Gupta, S.; Halladay, D.; Heil, J.; Heilig, J.; Hicke, B.; Husar, G.; Janjic, J.; Jarvis, T.; Jennings, S.; Katilius, E.; Keeney, T. R.; Kim, N.; Koch, T. H.; Kraemer, S.; Kroiss, L.; Le, N.; Levine, D.; Lindsey, W.; Lollo, B.; Mayfield, W.; Mehan, M.; Mehler, R.; Nelson, S. K.; Nelson, M.; Nieuwlandt, D.; Nikrad, M.; Ochsner, U.; Ostroff, R. M.; Otis, M.; Parker, T.; Pietrasiewicz, S.; Resnicow, D. I.; Rohloff, J.; Sanders, G.; Sattin, S.; Schneider, D.; Singer, B.; Stanton, M.; Sterkel, A.; Stewart, A.; Stratford, S.; Vaught, J. D.; Vrkljan, M.; Walker, J. J.; Watrobka, M.; Waugh, S.; Weiss, A.; Wilcox, S. K.; Wolfson, A.; Wolk, S. K.; Zhang, C.; Zichi, D. Aptamer-Based Multiplexed Proteomic Technology for Biomarker Discovery. *PLoS One* **2010**, *5*, No. e15004.
(15) Russell, T. M.; Green, L. S.; Rice, T.; Kruh-Garcia, N. A.; Dobos, K.; De Groote, M. A.; Hraha, T.; Sterling, D. G.; Janjic, N.; Ochsner, U. A. Potential of High-Affinity, Slow Off- Rate Modified Aptamer Reagents for Mycobacterium tuberculosis Proteins as Tools for Infection Models and Diagnostic Applications. *J. Clin. Microbiol.* **2017**, *55*, 3072−3088.
(16) Chen, C.; Zhou, S.; Cai, Y. Q.; Tang, F. Q. Nucleic acid aptamer application in diagnosis and therapy of colorectal cancer based on cell-SELEX technology. *npj Precis. Oncol.* **2017**, *1*, No. 37.
(17) Fish, A.; Vachani, A.; Beggs, M.; Carbonell, L.; Haddad, Z.; Juang, A.; Kamer, S.; Patel, B.; Yu, H.; Wu, A.; Massion, P.; Arjomandi, M.; Brown, J.; Trivedi, N.; Rubenstein, T. Risk Assessment for Indeterminate Pulmonary Nodules Using a Novel, Plasma-Protein Based Biomarker Assay. *J. Thorac. Oncol.* **2018**, *13*, S439.
(18) Rho, J. H.; Lampe, P. D. High-Throughput Analysis of Plasma Hybrid Markers for Early Detection of Cancers. *Proteomes* **2014**, *2*, 1−17.
(19) Mehan, M. R.; Williams, S. A.; Siegfried, J. M.; Bigbee, W. L.; Weissfeld, J. L.; Wilson, D. O.; Pass, H. I.; Rom, W. N.; Muley, T.; Meister, M.; Franklin, W.; Miller, Y. E.; Brody, E. N.; Ostroff, R. M. Validation of a blood protein signature for non-small cell lung cancer. *Clin. Proteomics* **2014**, *11*, No. 32.
(20) Kearney, P.; Hunsucker, S. W.; Li, X. J.; Porter, A.; Springmeyer, S.; Mazzone, P. An integrated risk predictor for pulmonary nodules. *PLoS One* **2017**, *12*, No. e0177635.
(21) Codreanu, S. G.; Hoeksema, M. D.; Slebos, R. J. C.; Zirnmerman, L. J.; Rahman, S. M. J.; Li, M.; Chen, S. C.; Chen, H. D.; Eisenberg, R.; Liebler, D. C.; Massion, P. P. Identification of Proteomic Features To Distinguish Benign Pulmonary Nodules from Lung Adenocarcinoma. *J. Proteome Res.* **2017**, *16*, 3266−3276.
(22) Li, X. J.; Hayward, C.; Fong, P. Y.; Dominguez, M.; Hunsucker, S. W.; Lee, L. W.; McLean, M.; Law, S.; Butler, H.; Schirm, M.; Gingras, O.; Lamontagne, J.; Allard, R.; Chelsky, D.; Price, N. D.; Lam, S.; Massion, P. P.; Pass, H.; Rom, W. N.; Vachani, A.; Fang, K. C.; Hood, L.; Kearney, P.; Blood-Based, A. A Blood-Based Proteomic Classifier for the Molecular Characterization of Pulmonary Nodules. *Sci. Transl. Med.* **2013**, *5*, No. 207ra142.
(23) Kikuchi, T.; Hassanein, M.; Amann, J. M.; Liu, Q. F.; Slebos, R. J. C.; Rahman, S. M. J.; Kaufman, J. M.; Zhang, X.; Hoeksema, M. D.; Harris, B. K.; Li, M.; Shyr, Y.; Gonzalez, A. L.; Zimmerman, L. J.; Liebler, D. C.; Massion, P. P.; Carbone, D. P. In-depth Proteomic Analysis of Nonsmall Cell Lung Cancer to Discover Molecular Targets and Candidate Biomarkers. *Mol. Cell. Proteomics* **2012**, *11*, 916−932.
(24) Rahman, S. M. J.; Ji, X. M.; Zimmerman, L. J.; Li, M.; Harris, B. K.; Hoeksema, M. D.; Trenary, I. A.; Zou, Y.; Qian, J.; Slebos, R. J. C.; Beane, J.; Spira, A.; Shyr, Y.; Eisenberg, R.; Liebler, D. C.; Young, J. D.; Massion, P. P. The airway epithelium undergoes metabolic reprogramming in individuals at high risk for lung cancer. *JCI Insight* **2016**, *1*, No. e88814.
(25) Rahman, S. M. J.; Gonzalez, A. L.; Li, M.; Seeley, E. H.; Zimmerman, L. J.; Zhang, X. Q. J.; Manier, M. L.; Olson, S. J.; Shah, R. N.; Miller, A. N.; Putnam, J. B.; Miller, Y. E.; Franklin, W. A.; Blot, W. J.; Carbone, D. P.; Shyr, Y.; Caprioli, R. M.; Massion, P. P. Lung Cancer Diagnosis from Proteomic Analysis of Preinvasive Lesions. *Cancer Res.* **2011**, *71*, 3009−3017.
(26) Yan, Y. L.; Marriott, G. Analysis of protein interactions using fluorescence technologies. *Curr. Opin. Chem. Biol.* **2003**, *7*, 635−640.
(27) Wienken, C. J.; Baaske, P.; Rothbauer, U.; Braun, D.; Duhr, S. Protein-binding assays in biological liquids using microscale thermophoresis. *Nat. Commun.* **2010**, *1*, No. 100.
(28) Lohse, M. J.; Nuber, S.; Hoffmann, C. Fluorescence/Bioluminescence Resonance Energy Transfer Techniques to Study G-Protein-Coupled Receptor Activation and Signaling. *Pharmacol. Rev.* **2012**, *64*, 299−336.
(29) Zhang, W.; Duhr, S.; Baaske, P.; Laue, E. Microscale thermophoresis for the assessment of nuclear protein-binding affinities. *Methods Mol. Biol.* **2014**, *1094*, 269−276.
(30) Wu, D. L.; Milutinovic, M. D.; Walt, D. R. Single molecule array (Simoa) assay with optimal antibody pairs for cytokine detection in human serum samples. *Analyst* **2015**, *140*, 6277−6282.
(31) Fichorova, R. N.; Richardson-Harman, N.; Alfano, M.; Belec, L.; Carbonneil, C.; Chen, S.; Cosentino, L.; Curtis, K.; Dezzutti, C. S.; Donoval, B.; Doncel, G. F.; Donaghay, M.; Grivel, J. C.; Guzman, E.; Hayes, M.; Herold, B.; Hillier, S.; Lackman-Smith, C.; Landay, A.; Margolis, L.; Mayer, K. H.; Pasicznyk, J. M.; Pallansch-Cokonis, M.; Poli, G.; Reicholderfer, P.; Roberts, P.; Rodriguez, I.; Saidi, H.; Sassi, R. R.; Shattock, R.; Cummins, J. E. Biological and technical variables affecting immunoassay recovery of cytokines from human serum and simulated vaginal fluid: A multicenter study. *Anal. Chem.* **2008**, *80*, 4741−4751.
(32) Rifai, N.; Ridker, P. M. High-sensitivity C-reactive protein: A novel and promising marker of coronary heart disease. *Clin. Chem.* **2001**, *47*, 403−411.
(33) Kammer, M. N.; Lakhani, D. A.; Balar, A. B.; Antic, S. L.; Kussrow, A. K.; Webster, R. L.; Mahapatra, S.; Barad, U.; Shah, C.; Atwater, T.; Diergaarde, B.; Qian, J.; Kaizer, A.; New, M.; Hirsch, E.; Feser, W. J.; Strong, J.; Rioth, M.; Miller, Y.; Balagurunathan, Y.; Rowe, D. J.; Helmey, S.; Chen, S. C.; Bauza, J.; Deppen, S. A.; Sandler, K.; Maldonado, F.; Spira, A.; Billatos, E.; Schabath, M. B.; Gillies, R. J.; Wilson, D. O.; Walker, R. C.; Landman, B.; Chen, H.; Grogan, E. L.; Baron, A. E.; Bornhop, D. J.; Massion, P. P. Integrated Biomarkers for the Management of Indeterminate Pulmonary Nodules. *Am. J. Respir. Crit. Care Med.* **2021**, *204*, 1306−1316.

https://doi.org/10.1021/acsomega.2c02763
ACS Omega 2022, 7, 31916−31923

(34) Kammer, M. N.; Kussrow, A.; Gandhi, I.; Drabek, R.; Batchelor, R. H.; Jackson, G. W.; Bornhop, D. J. Quantification of Opioids in Urine Using an Aptamer-Based Free-Solution Assay. *Anal. Chem.* **2019**, *91*, 10582−10588.
(35) Kammer, M.; Kussrow, A.; Carter, M. D.; Isenberg, S. L.; Johnson, R. C.; Batchelor, R. H.; Jackson, G. W.; Bornhop, D. J. Rapid quantification of two chemical nerve agent metabolites in serum. *Biosens. Bioelectron.* **2019**, *131*, 119−127.
(36) Baksh, M. M.; Kussrow, A. K.; Mileni, M.; Finn, M. G.; Bornhop, D. J. Label-free quantification of membrane-ligand interactions using backscattering interferometry. *Nat. Biotechnol.* **2011**, *29*, 357−U173.
(37) Saetear, P.; Perrin, A. J.; Bartholdson, S. J.; Wanaguru, M.; Kussrow, A.; Bornhop, D. J.; Wright, G. J. Quantification of Plasmodium-host protein interactions on intact, unmodified erythrocytes by back-scattering interferometry. *Malar. J.* **2015**, *14*, No. 88.
(38) Wang, M. M.; Kussrow, A. K.; Ocana, M. F.; Chabot, J. R.; Lepsy, C. S.; Bornhop, D. J.; O'Hara, D. M. Physiologically relevant binding affinity quantification of monoclonal antibody PF-00547659 to mucosal addressin cell adhesion molecule for in vitro in vivo correlation. *Br. J. Pharmacol.* **2017**, *174*, 70−81.
(39) Kammer, M. N.; Kussrow, A. K.; Olmsted, I. R.; Bornhop, D. J. A Highly Compensated Interferometer for Biochemical Analysis. *ACS Sens.* **2018**, *3*, 1546−1552.
(40) Bornhop, D. J.; Kammer, M. N.; Kussrow, A.; Flowers, R. A.; Meiler, J. Origin and prediction of free-solution interaction studies performed label-free. *Proc. Natl. Acad. Sci. U.S.A.* **2016**, *113*, E1595−E1604.
(41) Kammer, M. N.; Kussrow, A. K.; Bornhop, D. J. Longitudinal pixel averaging for improved compensation in backscattering interferometry. *Opt. Lett.* **2018**, *43*, 482−485.
(42) Markov, D.; Begari, D.; Bornhop, D. J. Breaking the 10(−7) barrier for RI measurements in nanoliter volumes. *Anal. Chem.* **2002**, *74*, 5438−5441.
(43) Swinney, K.; Markov, D.; Bornhop, D. J. Chip-scale universal detection based on backscatter interferometry. *Anal. Chem.* **2000**, *72*, 2690−2695.
(44) Tarigan, H. J.; Neill, P.; Kenmore, C. K.; Bornhop, D. J. Capillary-scale refractive index detection by interferometric backscatter. *Anal. Chem.* **1996**, *68*, 1762−1770.
(45) Kammer, M.; Kussrow, A. K.; Hoeksema, M.; Bornhop, D. J.; Massion, P. P. Performance Characteristics of CYFRA 21.1 Measurements by Compensated Backscattering Interferometry for the Early Detection of Lung Cancer. *Am. J. Respir. Crit. Care Med.* **2018**, No. 197.
(46) Kammer, M. N.; Olmsted, I. R.; Kussrow, A. K.; Morris, M. J.; Jackson, G. W.; Bornhop, D. J. Characterizing aptamer small molecule interactions with backscattering interferometry. *Analyst* **2014**, *139*, 5879−5884.
(47) He, A.; Liu, T. C.; Dong, Z. N.; Ren, Z. Q.; Hou, J. Y.; Li, M.; Wu, Y. S.; Novel, A. Immunoassay for the Quantization of CYFRA 21-1 in Human Serum. *J. Clin. Lab. Anal.* **2013**, *27*, 277−283.
(48) Muzyka, K. Current trends in the development of the electrochemiluminescent immunosensors. *Biosens. Bioelectron.* **2014**, *54*, 393−407.
(49) Hansson, L.; Hedner, T.; Dahlöf, B. Prospective randomized open blinded end-point (PROBE) study. A novel design for intervention trials. Prospective Randomized Open Blinded End-Point. *Blood Pressure* **1992**, *1*, 113−119.

https://doi.org/10.1021/acsomega.2c02763
ACS Omega 2022, 7, 31916−31923